energies

MDPI

Article

Research on Microscopic Pore Structure Characteristics and Influencing Factors of Shale Reservoirs: A Case Study of the Second Member of the Permian Lucaogou Formation in Malang Sag, Santanghu Basin

Xuejuan Zhang [1], Dandan Wang [2], Lei Zhang [1,*], Yabing Xing [1], Yi Zhang [1], Weiming Wang [3], Yinglin Liu [1] and Hongping Mao [1]

[1] School of Petroleum Engineering, Chongqing University of Science and Technology, Chongqing 401331, China
[2] Unconventional Oil and Gas Science and Technology Research Institute, China University of Petroleum (Beijing), Beijing 102249, China
[3] Unconventional Oil and Gas and New Energy Research Institute, China University of Petroleum (East China), Qingdao 266000, China
* Correspondence: zhlkeyan@163.com; Tel.: +86-177-2516-9619

Abstract: For the second member of the Permian Lucaogou Formation in Malang Sag, Santanghu Basin, we used field emission scanning electron microscopy (SEM), cryogenic nitrogen gas adsorption, and the micro/nano CT method, combined with the fractal theory, to depict the dense reservoir space types of the reservoir and the microcosmic pore structure characteristics, perform the quantitative evaluation of aperture size, pore shape, and connectivity, and to analyze the mineral composition of the micropore structure of the reservoir. The results show that the area is dominated by sandy/argillaceous dolomite, and the reservoir space types mainly develop dissolved intergranular pores and intergranular pores, a few microfractures, and parallel plate and slit nanoscale pores. There is a positive correlation between pore volume and specific surface area, with micropore volume accounting for 14.95%, mesopore volume at 82.47%, and macropore volume at 2.58%. The mesoporous volume provides the main pore storage space. The combined specific surface area of micropores and mesoporous pores accounts for more than 99% of the total specific surface area, providing almost all the pore surface area, which is the main site for shale oil and gas adsorption. The fractal dimension D value of the samples is between 2.39 and 2.49, and the pore distribution of shale is relatively uniform, mainly developing mesoporous pores. The specific surface area and average radius are positively correlated with the content of dolomite in mineral components. The results of the CT experiment also confirm that the pore throat of samples with high dolomite content is mostly a coarse tubular and banded distribution in three-dimensional space, with good connectivity.

Keywords: Santanghu Basin; Lucaogou Formation; microscopic pore structure; fractal characteristics

Citation: Zhang, X.; Wang, D.; Zhang, L.; Xing, Y.; Zhang, Y.; Wang, W.; Liu, Y.; Mao, H. Research on Microscopic Pore Structure Characteristics and Influencing Factors of Shale Reservoirs: A Case Study of the Second Member of the Permian Lucaogou Formation in Malang Sag, Santanghu Basin. *Energies* **2023**, *16*, 2453. https://doi.org/10.3390/en16052453

Academic Editor: Reza Rezaee

Received: 19 January 2023
Revised: 27 February 2023
Accepted: 1 March 2023
Published: 4 March 2023

1. Introduction

In recent years, the world petroleum industry has been transitioning from conventional oil and gas to unconventional oil and gas [1–3]. The output of unconventional oil and gas was close to 70 million tons in 2020, which marks China entering a new stage of unconventional oil and gas revolution and development [4–8]. With the gradual deepening understanding of the oil and gas bearing system of shale formations, a series of breakthroughs have been made in shale oil exploration and development. As the main storage medium of shale oil and gas, the pore structure characteristics of the shale strata affect the enrichment of shale oil and gas [9–13]. Therefore, the evaluation of microscopic pore structure characteristics and their influencing factors are an important index for shale reservoir evaluation. It is one of the hot topics in shale oil geology research, including pore morphology, distribution, size, configuration relationship, connectivity, and mineral

composition [14–20]. For the evaluation of shale reservoir pore structure, previous studies usually used a single experiment or a combination of experimental results. However, due to the influence of the experimental principle, the pore structure characteristics obtained from each experiment have advantages and disadvantages in characterization, and there are also problems in the splicing of various experimental results. Although a single experimental method can only reflect part of the pore structure characteristics of the reservoir, many scholars [15–19] have found that the reservoir in this area mainly develops mesopores. The low-temperature nitrogen adsorption experiment is the most favorable means to characterize mesoporous pore structure.

The Santanghu Basin in this study is the key block of shale oil exploration and development. Although breakthroughs have been made in exploration in recent years, more than 80 exploration wells in the Lucaogou Formation of Tiaohu-Malang Sag have been well demonstrated [21]. However, the mineral composition of the oil-bearing strata in this block is different from that of other shale oil reservoirs in China. The clay mineral content of tight reservoirs is low, and mainly composed of carbonate minerals and felsic minerals. The pore structure is relatively complex, which restricts the increase in shale oil in this area. Therefore, through the whole rock X-ray diffraction experiment, field emission scanning electron microscopy, low-temperature nitrogen adsorption, micro–nano CT, and other experimental methods, combined with fractal theory, the pore types and micropore structure characteristics of the tight reservoir space of the shale series in the study area were characterized, and the pore size, morphology, and connectivity were quantitatively evaluated. The correlation between the microscopic pore structure characteristics of the reservoir and the mineral composition was systematically analyzed. It is expected to provide a basis for shale oil and gas reservoir reconstruction and further exploration and development in the basin.

2. Geological Setting

The basin is located in northeast Xinjiang, with a NW–SE belt distribution (Figure 1a). The study area is located in the central and southern parts of the basin, and the provenance is mainly terrestrial input. During the whole deposition process, the lake basin area is large, the lake water depth is large, the water energy is low, and the stable and continuous deposition time is long [22]. On the whole, a set of lake transgression fine-grained deposits are deposited, and the developed lithology is carbonate rock, dark mudstone, argillaceous dolomite, calcareous dolomite, tuffaceous mudstone, tuffaceous siltstone, dolomitic mudstone, and so on, which are all developed in thin interbeds. Through the analysis of single-well data (Figure 1b), it can be seen that the span of organic matter content is large. The *TOC* value is 0~35%, and the average value is 6.3%. The measured value of *R*o is 0.5%~0.9%, and a small number of samples are more than 0.9%, which are all in the oil generation stage.

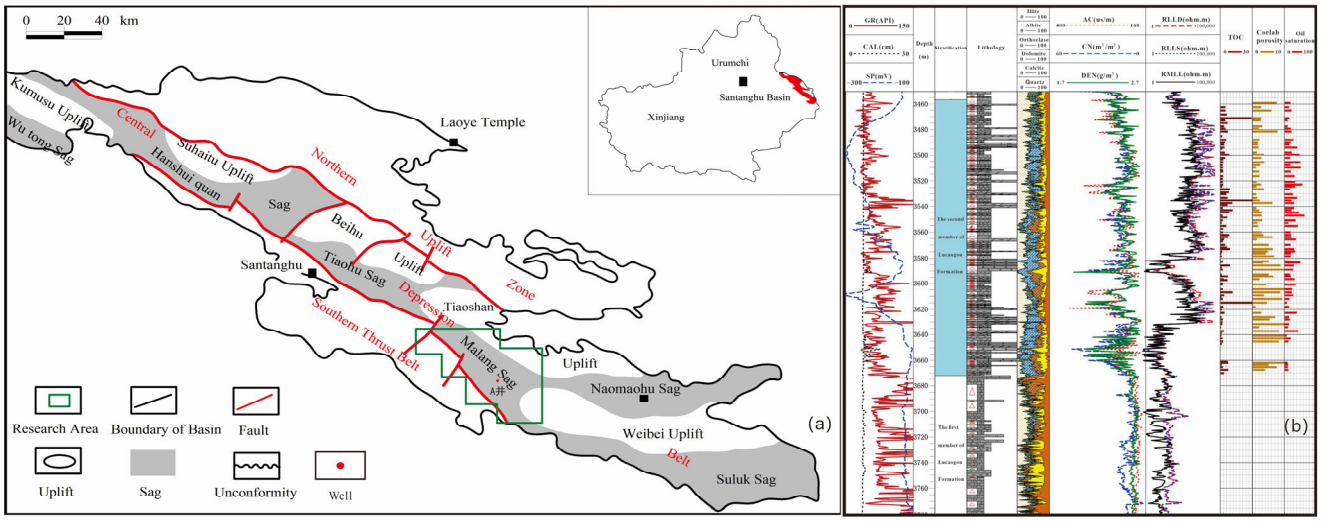

Figure 1. Geological background of Santanghu Basin; (**a**) Tectonic sketch of the basin and location of the study area (adapted from ref. [20]); (**b**) Single well histogram of well A.

3. Samples and Experimental Methods

3.1. Sample Collection

The samples were taken from well A of the shale reservoir in the second member of the Lucaogou Formation in the Malang Sag, Santanghu Basin. Due to the complex lithology changes during the sedimentary period in this area, the core of well A in the target area was observed, and a reasonable sampling scheme has been designed to ensure the representativeness of the experimental samples. Twenty-four samples were taken in total.

The selected samples have been analyzed by X-ray diffraction to determine the mineral composition and content of the samples. Twelve samples with different mineral compositions were selected for argon ion polishing, and field emission scanning electron microscopy was performed, based on this, to qualitatively determine the pore type of the shale reservoir space. Eight samples were selected for low-temperature nitrogen adsorption experiments to quantitatively determine the morphology and pore size of micropores in shale reservoirs. On this basis, three samples were selected for micro–nano CT experiments to clarify the connectivity of micropores in shale reservoirs.

3.2. Experimental Instruments and Lab Analysis

3.2.1. X-ray Diffraction Analysis

The whole rock quantitative X-ray diffraction analysis adopts a D8-DISCOVER X-ray diffractometer. The experimental standard refers to the SY/T 5163-2018 analytical method for clay minerals and common nonclay minerals in shale rocks by X-ray diffraction. Before the experiment, the samples were treated with oil washing, low-temperature drying, grinding, etc. The test temperature was 27 °C and the ambient humidity was 40%. The sample to be tested was ground to 320 mesh powder, 3~5 g, and the treated powder was evenly applied to the glass carrier sheet. The parameters of the emission spectrum line were set and the experiment was carried out. The sample detection angle was generally set to 10~90°. We collected the sample diffraction spectrum line, then analyzed the spectrum line and analyzed its mineral composition.

3.2.2. Micro–Nano CT Experiment

This experiment was based on the 'unconventional oil and gas accumulation and development' national key laboratory cultivation base and the GE Phoenix Nanotom S digital core analysis system in Northeast Petroleum University. The instruments and models used were the GE Phoenix nano tom S Germany universal nanometer X-ray digital

core analysis systems. A 2 mm diameter drill bit was used to drill the core samples, which were placed in a GE Phoenix Nanotom S nano-CT device and scanned by adjusting the device parameters. The scanned data were used to reconstruct the digital 3D model with GE Phoenix Datosx 2 Acq X software. Then the professional data processing software AVIZO 8.0 was used to analyze and process the reconstructed three-dimensional digital model, display the three-dimensional internal view, extract the core pores, and analyze them. The scanning accuracy of core samples is 1.06 μm.

3.2.3. Nitrogen Adsorption Experiment

The nitrogen adsorption experiment adopted the ASAP2460 adsorption instrument of the Mack Company in the United States. The aperture measurement range of the instrument was 0.35–500 nm; the minimum specific surface area can be measured to 0.0001 m^2/g, and the minimum pore volume can be measured to 0.0001 cm^3/g. Before the experiment, the sample was placed in deionized water for ultrasonic cleaning, and the surface impurities were fully removed for low-temperature drying pretreatment and then were ground to 20–50 meshes. The powder sample was vacuumized at 120 °C for 12 h. Liquid nitrogen with a purity of greater than 99.99% was used as the adsorption medium and the experiment was carried out at −195.85 °C liquid nitrogen temperature.

3.2.4. SEM Experiment

In the scanning electron microscope (SEM) experiment, a Czech TESCAN VEGE field emission scanning electron microscope was used. The sample was polished to the size of the thumb with sandpaper, polished with argon ion, and then sprayed with gold by an ion sputtering instrument. The samples were observed in a field emission scanning electron microscope and the trace (mineral) elements were identified by an energy spectrometer. This study mainly studies the pore space development position and pore type of shale samples in the second member of the Lucaogou Formation.

3.3. Calculation Model of Fractal Dimension

The pore surface of shale has fractal characteristics. The microscopic pore structure characteristics of the shale reservoir can be expressed indirectly by fractal dimension, and its value D is between 2 and 3. When D is close to 2, the pore surface is smooth, and when D is close to 3, the pore surface is very rough [23–27]. The fractal dimension qualitatively reflects the uniformity of pore development. Micropores, mesopores, and macropores are developed, and the pore size distribution span is large. If only one pore is developed, that is, the pore volume and specific surface area are only provided by one type of pore, then the fractal dimension is small. The fractal dimension has different effects on the occurrence and migration of oil and gas. The larger the fractal dimension is, the more complex the pore structure is, which is beneficial to oil and gas adsorption and storage, but not conducive to oil and gas seepage. The commonly used method to calculate the fractal dimension is the FHH equation, Formula (1).

$$\ln V = (D - 3) \ln[\ln (P_0/P)] + C \quad (1)$$

In the formula, V is gas adsorption capacity, cm^3/g; P is the system balance pressure, Mpa; P_0 is the saturated vapor pressure of adsorbed gas, MPa; C is a constant; D is the fractal dimension of porous materials.

4. Results

4.1. Rock Mineral Composition Characteristics of Shale Reservoirs

The clay mineral content was low; the average content was 12.45%, and it was mainly feldspar minerals and carbonate minerals, quartz, potash feldspar, and albite, with a maximum quartz content of 46.879% and an average value of 23.104%. The maximum potassium feldspar content was 30.701%, with an average of 14.439%; the maximum albite content was 38.606%, with an average of 12.890%; carbonate minerals were mainly dolomite

and calcite, and the maximum calcite content was 35.711%, and the average was 10.051%; the maximum content of dolomite was 53.317%, and the average content was 24.916%. There were also some secondary minerals such as pyrite and siderite. The maximum content of pyrite was 2.093%, and the average content was 0.675%. The maximum content of siderite was 2.984%, with an average of 1.502% (Figure 2a,b). According to the mineral composition characteristics of the area, the rock types in the shale reservoirs in the Lucaogou Formation were divided by using the classification scheme of the four-component three-terminal element of literature [22], with the content of carbonate rock, the total content of quartz and feldspar, and the content of clay minerals as three-terminal elements. The rock types in this area were mainly argillaceous dolomite, composed of microcrystalline dolomite and a small number of clay minerals, followed by sandy dolomite, which was composed of microcrystalline dolomite and a small amount of quartz, albite, and other minerals; it contained only a very small amount of dolomitic siltstone dolomitic mudstone (Figure 2c).

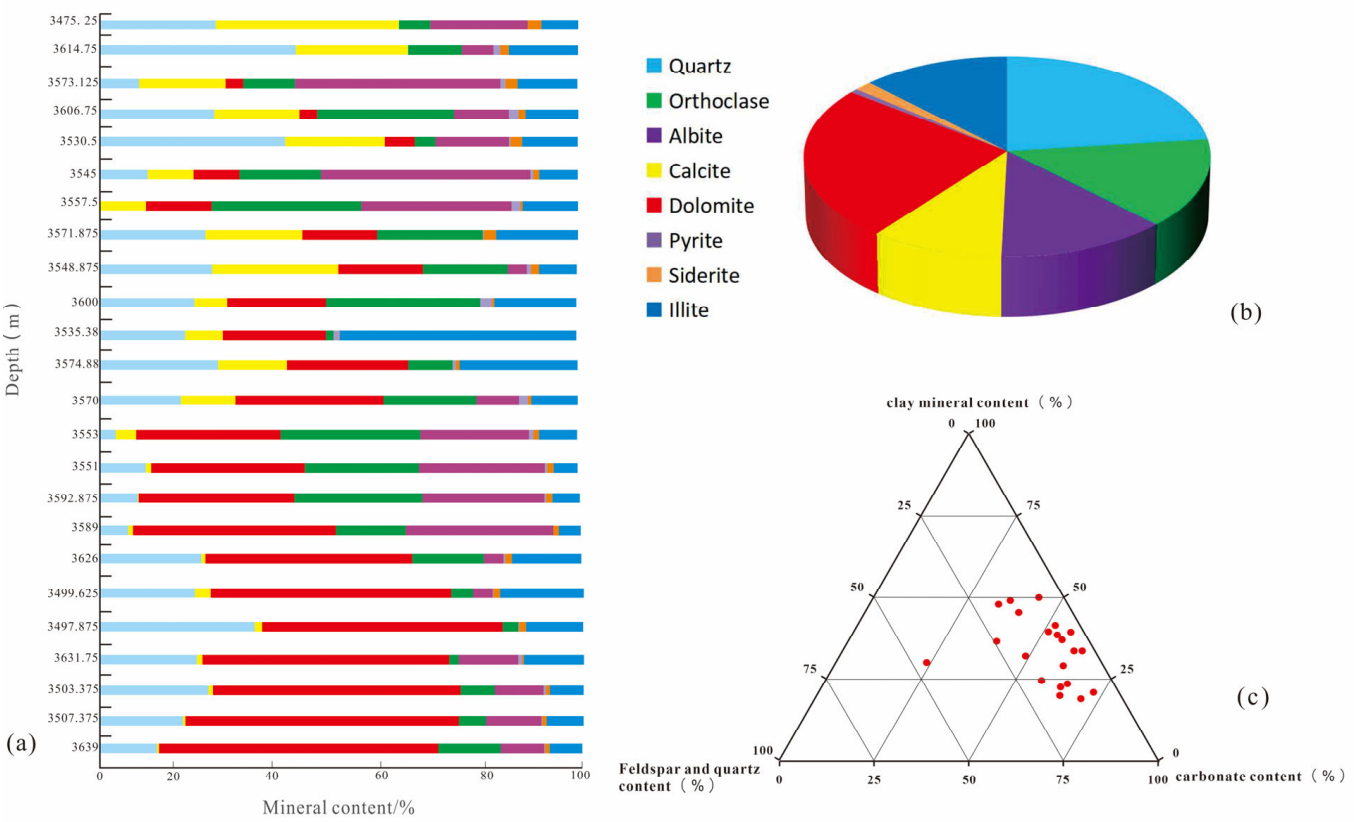

Figure 2. Mineral composition and rock type of shale. (**a**) Vertical distribution of mineral composition; (**b**) Planar distribution of mineral composition; (**c**) Classification of rock types.

4.2. Characteristics of Pore Types in Shale Reservoir Space

Through the observation of sub-ion profiling and field emission scanning electron microscopy on twelve rock samples, the results show (Figure 3) that, under the strong compaction and cementation, the primary pores in this area have basically disappeared, but the secondary pores are relatively developed in carbonate minerals and clay minerals. Most of them are selective dissolution of feldspar and clay minerals by pore fluid [27–31], forming intragranular dissolution pores in particles or intergranular dissolution pores between particles. According to the classification scheme proposed by LOUCKS et al. for shale reservoirs [27–30], the pore types of the second member of the Lucaogou Formation can be divided into mineral matrix pores (intergranular pores, intragranular pores), organic pores, and fractures.

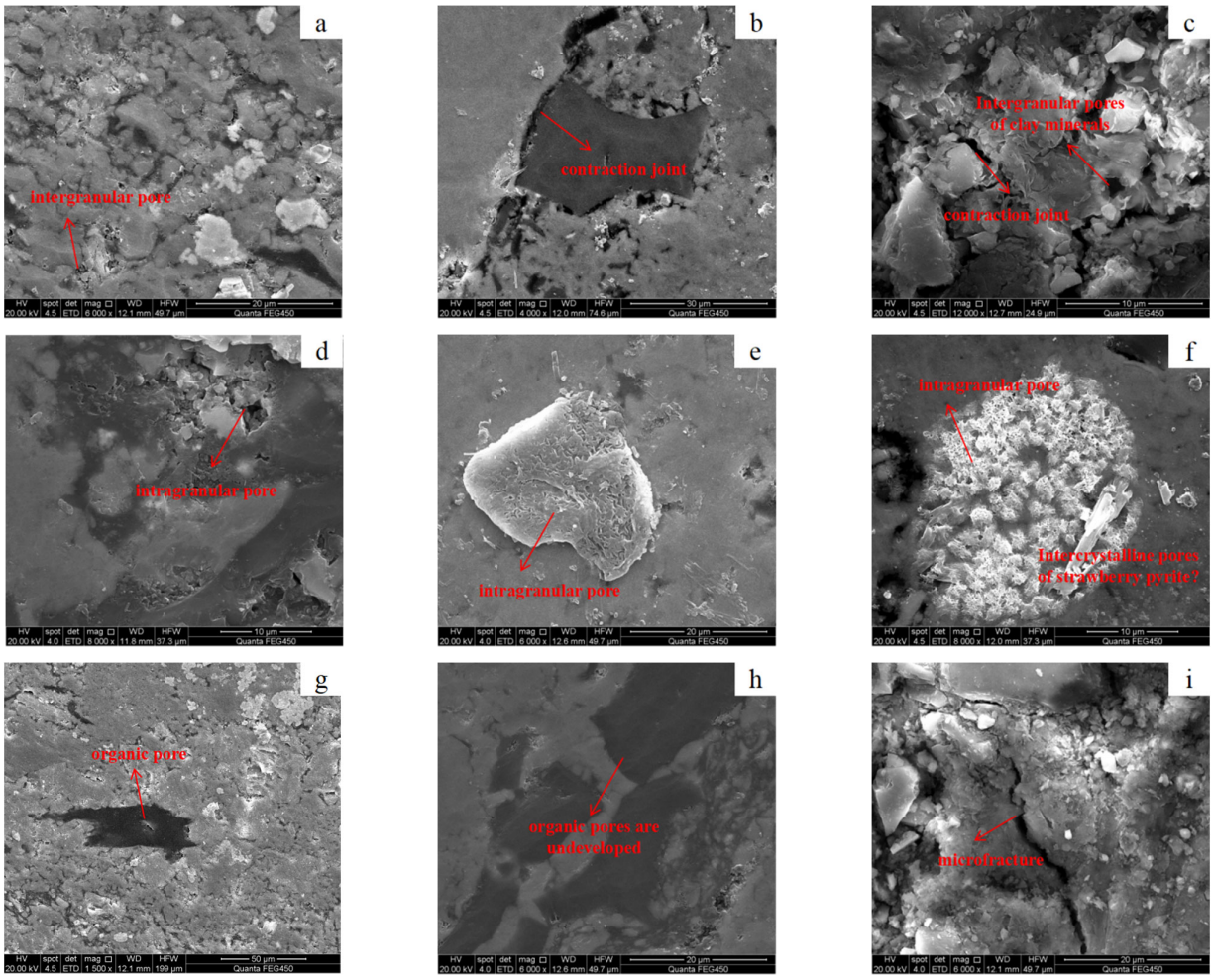

Figure 3. Reservoir space types of the second member of the Lucaogou Formation. (**a**) Intergranular pores (3599.98 m, dolomite content 15.758%); (**b**) Intergranular pores/edge contraction joints (3638.98 m, 53.317%); (**c**) Intergranular pores/marginal contraction sutures (3670 m, 38.2%); (**d**) Intergranular pores and intragranular pores (3614.81 m, 0%); (**e**) Intragranular pores (3503.41 m, 47.893%); (**f**) Intragranular pores (3638.98 m, 53.317%); (**g**) Organic pores (3599.98 m, 15.758%); (**h**) Organic pores (3574.87 m, 22.541%); (**i**) Microcracks (3589.04 m, 37.686%).

Mineral matrix pores are mainly intergranular pores and intragranular pores. The main causes are the narrow and long irregular pores along the mineral edge formed by the volume shrinkage of dolomite crystals during dolomitization, and the pores produced by the dissolution of carbonate rocks through acidic fluids generated during the hydrocarbon generation of organic matter. The rock of the second member of the Lucaogou formation is dense as a whole, and the intergranular pores are scattered among the skeleton mineral particles. The edge fractures are more developed, such as in Figure 3a,b. The intergranular pores in the clay mineral aggregate are mostly lamellar, as shown in Figure 3c, and the pore size difference is obvious and mostly micron grade. Most of the intragranular pores are secondary dissolved pores formed by the dissolution of mineral particles, and the distribution is more concentrated, such as in Figure 3d,e. There are also intragranular pores in pyrite aggregates, such as in Figure 3f. The dissolved pores are mostly round and oval, and the pore size varies greatly. The connectivity of pores are related to the development degree of dissolution. The stronger the pore dissolution, the easier it is to form a pore network with excellent connectivity. The organic matter in this section was relatively developed, but the development of organic matter pores are rarely shown in Figure 3g,h. The development of microcracks in this layer are shown in Figure 3i.

4.3. Microstructure Characteristics of Shale Reservoirs

The basic principle of low-temperature nitrogen adsorption is that, at low temperatures, nitrogen will be physically adsorbed on the surface of the sample. With the increase in pressure, the monolayer adsorption gradually reaches multilayer adsorption, and capillary condensation occurs when the corresponding pore size reaches the critical pressure. Then, gradually reducing the partial pressure, the adsorbed nitrogen begins to desorb. The adsorption isotherms of eight samples showed an inverse 'S' type (Figure 4). The adsorption–desorption curves of typical mesoporous materials proposed by SING were the same [22]. The desorption isotherm of the sample was located above the adsorption isotherm, which did not overlap and formed a hysteresis loop.

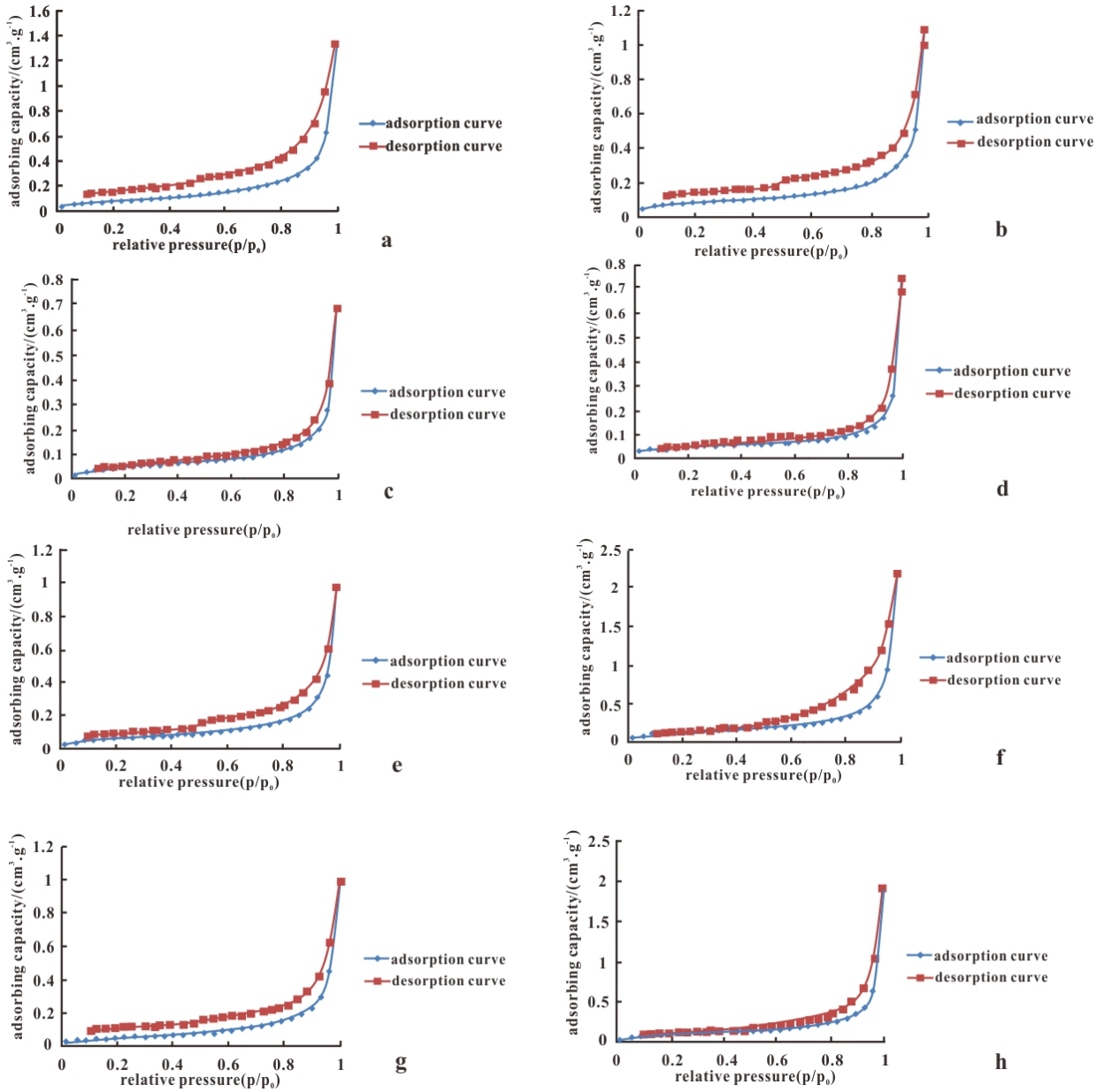

Figure 4. Adsorption and desorption curves of shale samples in the study area. (**a**) L1 sample, dolomite content 0%; (**b**) L2 sample, dolomite content 5.462%; (**c**) L3 sample, dolomite content 15.758%; (**d**) L4 sample, dolomite content 22.54%; (**e**) L5 sample, dolomite content 26.058%; (**f**) L6 sample, dolomite content 32.431%; (**g**) L7 sample, dolomite content 43.082%; (**h**) L8 sample, dolomite content 53.317%.

The hysteresis loops were reclassified by IUPAC in 2015 [26] (Table 1). The shale samples in this area were mainly H3 and H4 hysteresis loops (Figure 4). The adsorption curve and desorption curve increased slowly. When the relative pressure was large, the adsorption capacity began to increase rapidly, and the hysteresis loops were small as a whole, reflecting the open parallel plate pores and slit pores around. The pores in each pore section from micropore to macropore were well developed. The adsorption curve and desorption curve of a few samples were nearly coincident, and the hysteresis loop was small. The degree of pore opening was relatively high, and the pore connectivity was good. This pore structure was beneficial to the migration of shale oil and gas.

Table 1. IUPAC 2015 hysteresis classification.

H1	H2
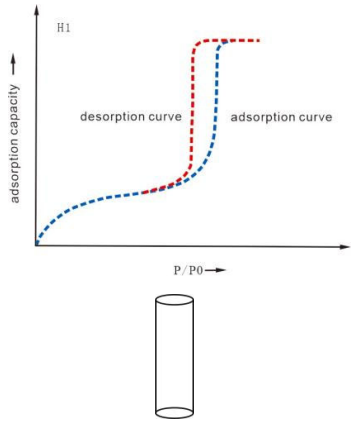	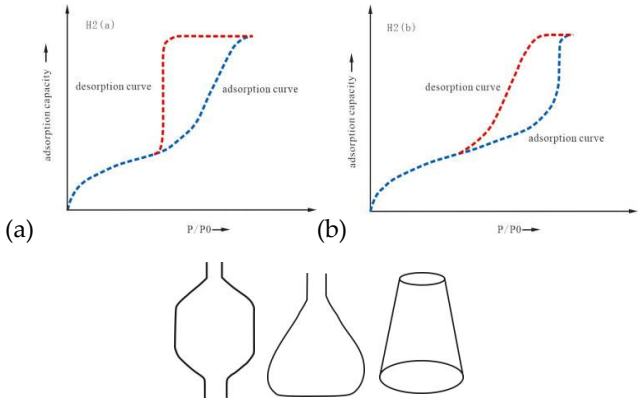
H3	**H4**
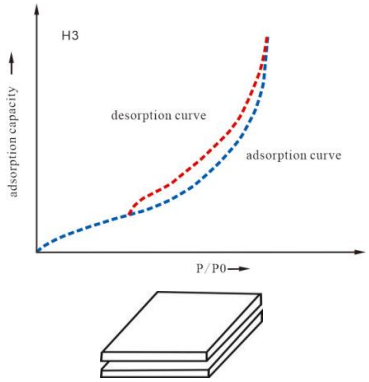	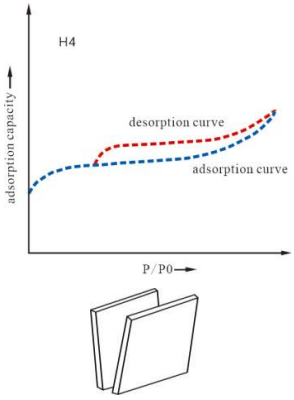

The calculation results of surface area, pore volume, and pore size (Table 2) showed that the specific surface area of 8 samples was 0.1410~0.4510 m^2/g, and the average specific surface area was 0.2668 m^2/g. The pore volume was 1.057~2.961 $\times 10^{-3}$ cm^3/g and the average pore volume was 1.9094 $\times 10^{-3}$ cm^3/g. At present, there is no unified understanding of the classification of shale pores at home and abroad, but it is more common to use the IUPAC pore classification method: microporous (pore diameter is less than 2 nm), mesoporous (pore diameter is between 2 and 50 nm), and macropores (pore diameter is greater than 50 nm). The specific surface area and pore volume of shale samples in the study area were small, and there was little pore development. The specific surface area density of samples was mainly distributed below 50 nm. The specific surface areas of micropores, mesopores, and macropores accounted for 32.67%, 67.15%, and 0.18% of the total specific surface areas, respectively. The specific surface area of micropores and mesopores in shale accounted for more than 99% of the total specific surface area, indi-

cating that micropores and mesopores with pore diameter less than 50 nm provide most of the pore specific surface area, and were the main sites for shale oil and gas adsorption. The pore volume density distribution was bimodal. The main peak of 8~20 nm was 28~43 nm (Figures 5 and 6). The micropore volume of shale samples accounted for 14.95%, the mesopore volume accounted for 82.47%, and the macropore volume accounted for 2.58%, which further confirmed that the mesopore provided the main pore storage space, and the contribution of micropores and macropores was less. The main pore size was 28~43 nm.

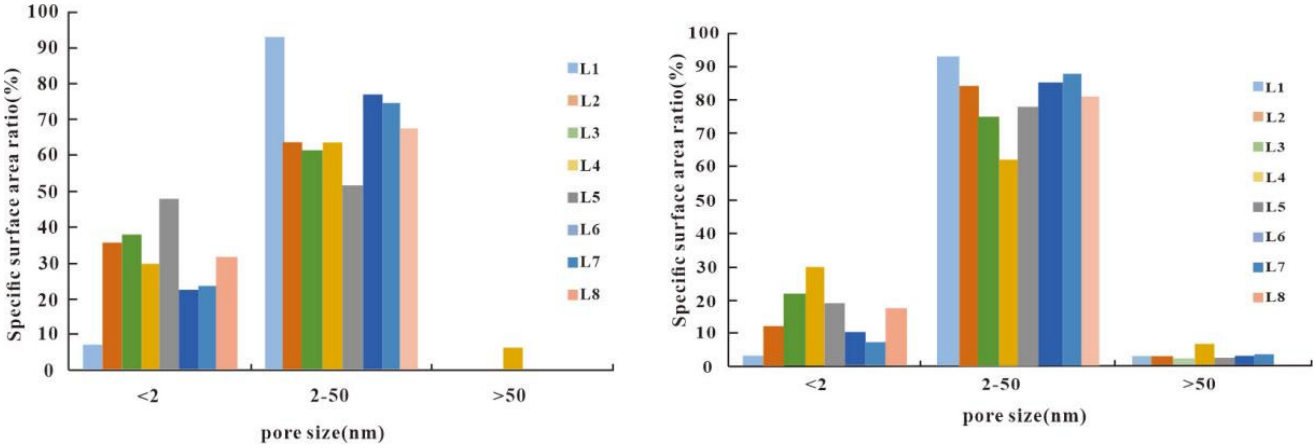

Figure 5. Specific surface area distribution and pore volume distribution of Lucaogou Formation shale in Malang Sag, Santanghu Basin.

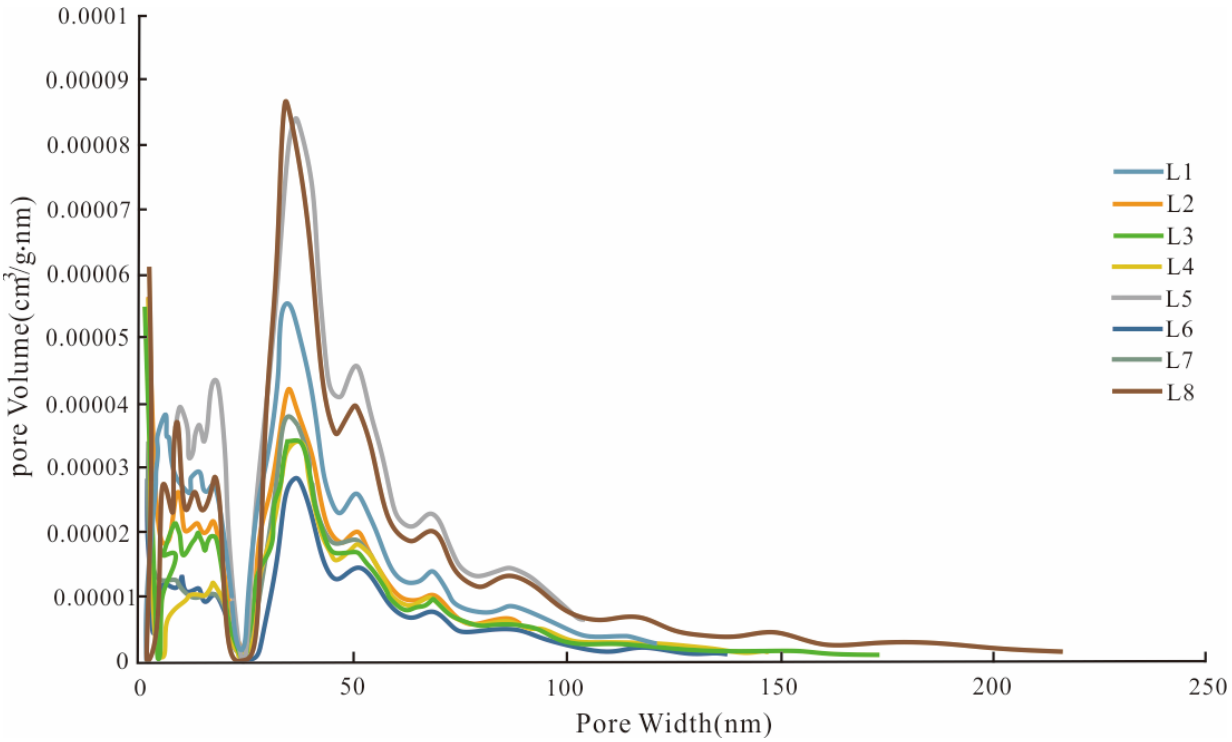

Figure 6. Shale pore size distribution map of Lucaogou Formation in Malang Sag, Santanghu Basin.

Table 2. Pore structure parameter table of shale samples.

Samples	Specific Surface Area ($m^2 \cdot g^{-1}$)	Average Pore Diameter (nm)	Total Pore Volume ($cm^3 \cdot g^{-1}$)
L1	0.2972	14.1670	2.060
L2	0.2547	16.2743	1.620
L3	0.1794	19.9069	1.057
L4	0.1410	27.4237	1.144
L5	0.2369	16.2914	1.512
L6	0.4510	15.7213	3.422
L7	0.2077	18.1771	1.499
L8	0.3664	25.2121	2.961

4.4. Micropore Connectivity of Shale Reservoir

CT scanning technology obtained the characteristic slices of the microscopic pore structure of tight reservoirs at different scales by multi-scale non-destructive scanning imaging of the same sample. Then, the gray image was binarized and segmented by the Avizo software filtering, three-dimensional reconstruction, and image segmentation functions. The pore and particle-matrix were divided, and the binarized segmentation image (Figure 7) was obtained. The structured pore and throat models were extracted for three-dimensional reconstruction to analyze the spatial distribution characteristics and connectivity characteristics of shale pores.

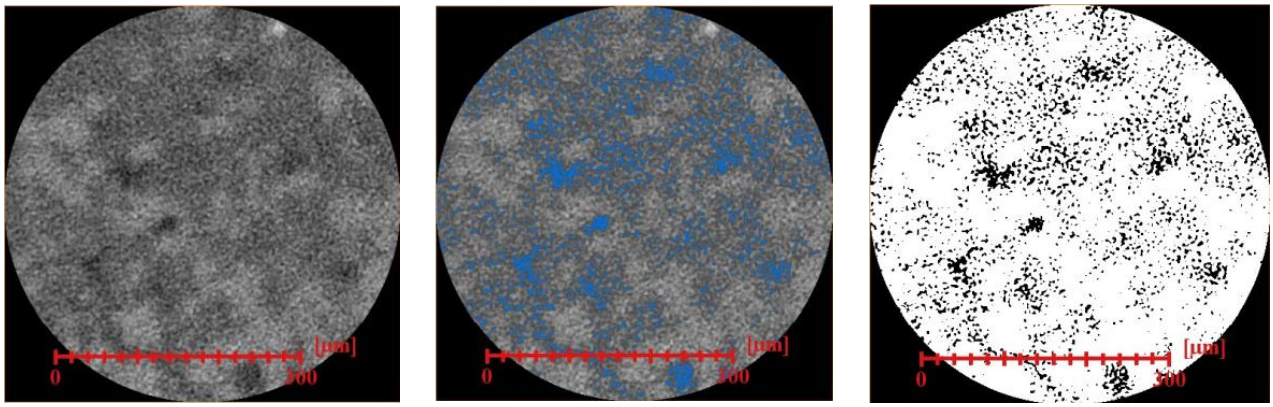

Figure 7. CT image processing result process.

Micro–nano CT experiments were carried out on three samples with dolomite content of 0%, 26.058%, and 53.317%, numbered L1, L5, and L8. After comparing the data obtained by pore extraction, we can find that (Table 3): The comparison showed that, from L1 to L5 and L8, the contact relationship between particles became looser and looser (Figure 8a,b), the dissolved pores between strip particles gradually increased, the dissolved pores in isolated particles gradually decreased, the connectivity gradually improved, and the throat became larger and larger. The pore throats of the L8 samples with high dolomite content were mostly coarse tubular and banded distributions in three-dimensional space, and the distribution was uniform. There were 67.85% of throats with good connectivity. The average pore radius was 3.09 μm, the throat length was 47.20 μm, the number of identified pores was 55,555, and the pore volume was 9,174,542.24 $\mu m^3/g$ (Table 3). The pore throats of samples with dolomite content of 26.058% were mostly banded and spherical in three-dimensional space. The pore throats of the L1 sample with the lowest dolomite content was mostly isolated and spherical in three-dimensional space. The number of identified pores was 6674, the average pore radius was 1.85 μm, and the throat length was 8.67 μm. Only 0.46% of the throats had good connectivity. It can be seen that dolomite content has an impact on pore structure. High dolomite content mainly plays a supporting role in the

reservoir, preventing compaction, improving pore structure, and increasing the connectivity of micropores.

Table 3. Shale pore structure distribution parameters of Lucaogou Formation in Malang Sag, Santanghu Basin.

Sample Number	Scanning Resolution/μm	Calculate Porosity/%	Average Pore Radius/μm	Number of Pores	Pore Volume/μm^3	Throat Average Length/μm	Connected Volume Percentage/%
L1	0.95	1.84	1.85	6674	248,164.56	8.67	0.46
L5	0.97	4.60	4.92	13,033	996,556.63	18.74	16.22
L8	0.97	11.92	3.09	55,555	9,174,542.24	47.20	67.85

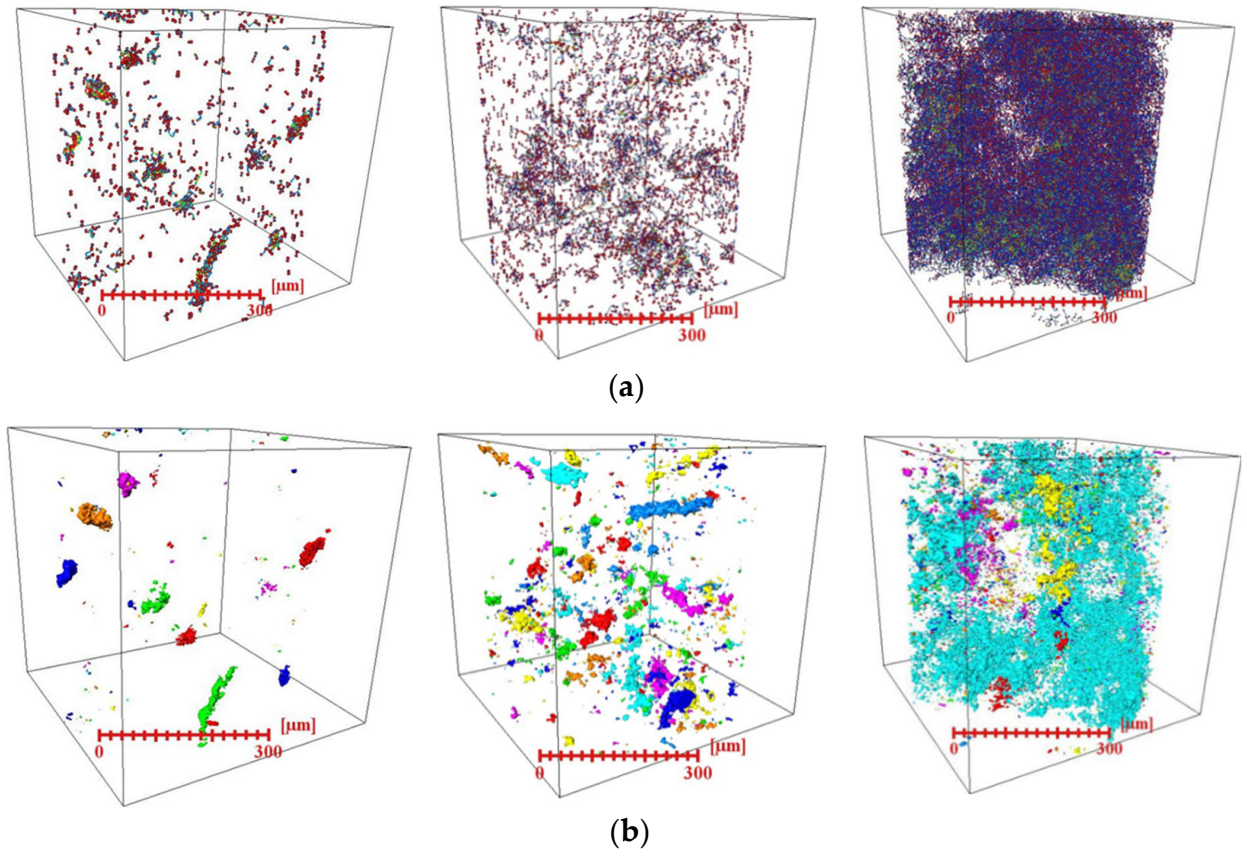

Figure 8. CT experimental pore throat distribution and connectivity map of Lucaogou Formation shale in Malang Sag, Santanghu Basin. (**a**) Spatial distribution map of pore throats of Lucaogou Formation shale in Malang Sag, Santanghu Basin. (**b**) Shale pore space connectivity map of Lucaogou Formation in Malang Sag, Santanghu Basin.

5. Discussion

5.1. Fractal Dimension of Shale Pore

According to the measured nitrogen adsorption isotherm, the fractal fitting curve of LnV on Ln[Ln(P_0/P)] was made, such as in Figure 9. Table 4 shows the fractal dimension of shale samples calculated by the slope of the fractal fitting line. The correlation coefficient R^2 of the linear fitting was above 0.96, indicating that shale pores have fractal characteristics. The fractal dimension D of shale was between 2.41 and 2.49, and the value was closer to 2, indicating that shale pores were evenly distributed and were mainly developed as mesopores, which is conducive to the reservoir and migration of oil and gas.

Table 4. Fitting parameters of fractal FHH model for nitrogen adsorption.

Sample Number	Fractal Fitting Equation	Correlation Coefficient	Fractal Dimension
L1	$y = -0.5891x - 2.303$	0.9933	2.4109
L2	$y = -0.5421x - 2.4531$	0.9939	2.4579
L3	$y = -0.5236x - 2.8818$	0.9778	2.4764
L4	$y = -0.5273x - 3.1073$	0.9667	2.4727
L5	$y = -0.5134x - 2.5294$	0.9941	2.4866
L6	$y = -0.5618x - 1.9388$	0.9894	2.4382
L7	$y = -0.5621x - 2.6621$	0.9937	2.4379
L8	$y = -0.5623x - 2.1949$	0.978	2.4377

5.2. Effect of Mineral Composition on Microscopic Pore Structure

Previous studies have shown that the microscopic pore structure of shale is closely related to its material composition. Organic matter, clay minerals, carbonate minerals, quartz, and feldspar greatly affect the microscopic pore structure of shale [32]. There is a good positive correlation between pore volume and specific surface area (Figure 10a); the correlation coefficient is 0.9575, indicating that mesopores play a dominant role in the pore system, which can provide both specific surface area and pore volume. The fractal dimension was mainly negatively correlated with the specific surface area (Figure 10b). It indicates that the larger the specific surface area is, the smaller the fractal dimension is, and the pores tend to be uniform. Through the correlation analysis of the mineral content and specific surface area, pore volume, and average pore diameter of the second member of the Lucaogou Formation, it can be seen that, in the mineral composition, the dolomite content is positively correlated with the specific surface area and the average radius (Figure 10c), indicating that the intergranular and intragranular dissolved pores associated with dolomite are relatively developed and mainly mesoporous. With the increase in dolomite content, the number of pores and pore diameters increase. The specific surface area was negatively correlated with the content of illite, and the average radius was positively correlated with it (Figure 10d), indicating that the clay mineral illite was mainly corroded, mainly contributing to the macropores formed by corrosion and increasing the pore size. The feldspar content is negatively correlated with the average radius (Figure 10e), indicating that the feldspar has less corrosion and mainly fills the pores, resulting in a decrease in pore size. In summary, the higher the dolomite content, the more developed the pores, the larger the diameter of pores and throats, and the better the connectivity. It can be inferred that the relatively enriched dolomite is the main enriched layer of shale oil.

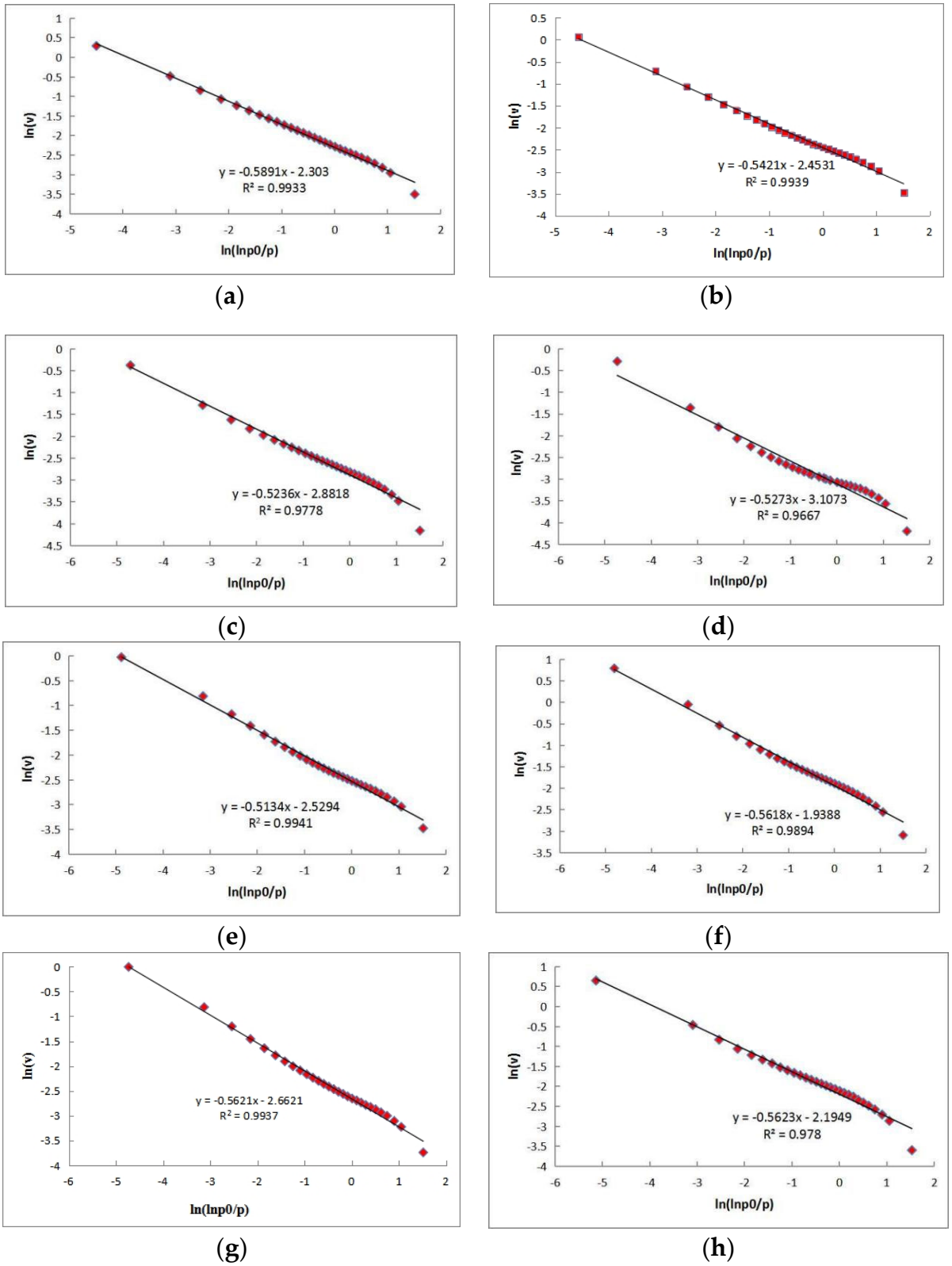

Figure 9. Fractal dimension of shale samples in the study area. (**a**) L1 sample, dolomite content 0%; (**b**) L2 sample, dolomite content 5.462%; (**c**) L3 sample, dolomite content 15.758%; (**d**) L4 sample, dolomite content 22.54%; (**e**) L5 sample, dolomite content 26.058%; (**f**) L6 sample, dolomite content 32.431%; (**g**) L7 sample, dolomite content 43.082%; (**h**) L8 sample, dolomite content 53.317%.

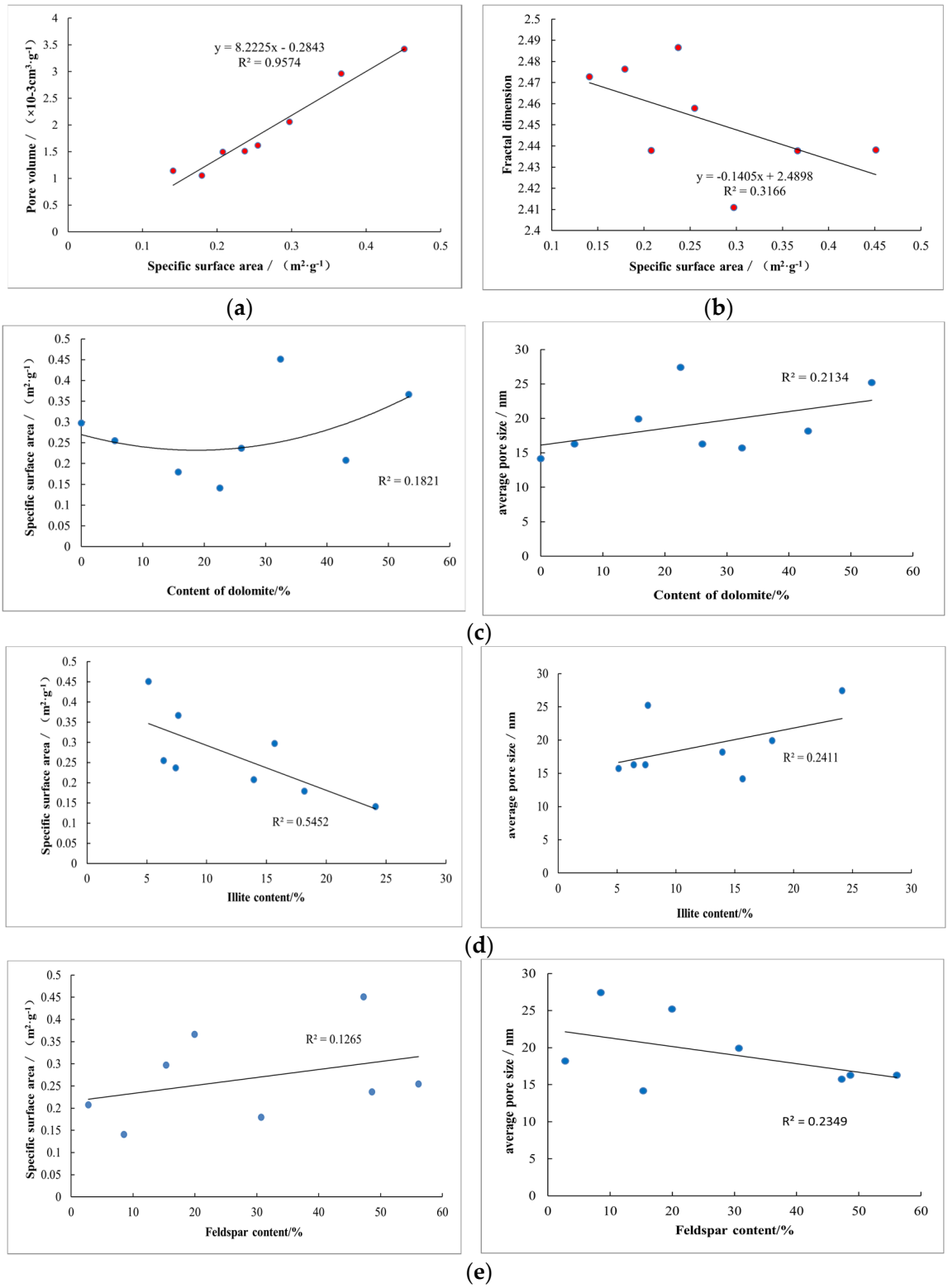

Figure 10. Correlation diagram between pore structure parameters and control factors of the second member of Lucaogou Formation. (**a**) Relationship between specific surface area and pore volume; (**b**) Relationship between specific surface area and fractal dimension; (**c**) Relationship between dolomite content and specific surface area and average pore size; (**d**) Relationship between illite content and specific surface area and average pore size; (**e**) Relationship between feldspar content and average pore size and specific surface area.

6. Conclusions

1. The mineral composition of shale reservoirs in the study area is dominated by quartz and carbonate minerals, and sandy/argillaceous micritic dolomite is mainly developed. The pore types are mainly intergranular pores of brittle minerals, marginal fractures, intergranular dissolved pores formed by dissolution of carbonate minerals, intragranular dissolved pores, and nano-scale pore throat systems. H3 and H4 hysteresis loops are developed.
2. The specific surface area and pore volumes were small. Micropore volume accounted for 14.95%, mesopore volume accounted for 82.47%, and macropore volume accounted for 2.58%. Mesopores provided the main reservoir space. The specific surface area of micropores, mesopores, and macropores accounted for 32.67%, 67.15%, and 0.18% of the total surface area, respectively. The specific surface areas of micropores and mesopores accounted for more than 99% of the total specific surface areas. Micropores and mesopores with pore diameters less than 50 nm provided most of the pore-specific surface areas, which are the main sites for shale oil and gas adsorption. The fractal dimension D value is between 2.41 and 2.49, and the value is closer to 2, indicating that shale pore distribution is more uniform, mainly for mesoporous pore development.
3. The pore volume increases with the increase in specific surface area. In the mineral composition, illite content is negatively correlated with specific surface area and positively correlated with average radius, and feldspar content is negatively correlated with average radius. Clay minerals have undergone a large amount of dissolution, mainly developing macropores and increasing pore size. However, feldspar dissolution is less, and it mainly fills pores. The dolomite content is positively correlated with the specific surface area and the average radius. The higher the dolomite content, the more developed the pores, and the specific surface area and pore size are provided. The pore throats of the samples with high dolomite content are mostly coarse tubular and banded in three-dimensional space, and the connectivity is also good.

Author Contributions: Conceptualization, Y.L. and H.M.; methodology, L.Z.; software, D.W.; formal analysis, Y.Z.; investigation, Y.X.; data curation, W.W.; writing—original draft preparation, X.Z. All authors have read and agreed to the published version of the manuscript.

Funding: This research was funded by the Natural Science Foundation of Chongqing, China, grant number cstc2020jcyj-msxmX0657, cstc2021jcyj-msxmX0984, and the National Natural Science Foundation of China, grant number 41672113.

Data Availability Statement: Not applicable.

Conflicts of Interest: The funders had no role in the design of the study; in the collection, analyses, or interpretation of data; in the writing of the manuscript; or in the decision to publish the results.

References

1. Zou, C.N.; Zhu, R.K.; Wu, S.T.; Yang, Z.; Tao, S.Z.; Yuan, X.J.; Hou, L.; Yang, H.; Xu, C.; Wang, L.; et al. Types, characteristics, mechanisms and prospects of conventional and unconventional hydrocarbon accumulation—Taking China's tight oil and gas as an example. *J. Pet.* **2012**, *33*, 173–187.
2. Jia, C.Z.; Zheng, M.; Zhang, Y.F. China's unconventional oil and gas resources and exploration and development prospects. *Pet. Explor. Dev.* **2012**, *39*, 129–136. [CrossRef]
3. Zou, C.N.; Yang, Z.; Cui, J.W.; Zhu, R.K.; Hou, L.H.; Tao, S.Z.; Yuan, X.; Wu, S.; Lin, S.; Yao, J.L.; et al. Formation mechanism, geological characteristics and development countermeasures of shale oil. *Pet. Explor. Dev.* **2013**, *40*, 14–26. [CrossRef]
4. Jiang, F.J.; Pang, X.Q.; Ouyang, X.C.; Guo, J.; Jin, C.; Huo, Z.; Wang, Q. Overview of world shale gas research and potential analysis of shale gas resources in China. *Geol. Front.* **2012**, *19*, 198–211.
5. Zou, C.N.; Qiu, Z. The new progress of unconventional oil and gas sedimentology in China. *J. Sedimentol.* **2021**, *39*, 1–9.
6. Zou, C.N.; Zou, C.N.; Yang, Z.; Zhu, R.; Chen, X.; Zhang, X. The important progress of continental petroleum geology theory in central and western basins of China. *Oil Explor. Dev.* **2018**, *45*, 546–560.
7. Zhao, W.Z.; Hu, S.Y.; Hou, L.H.; Yang, T.; Li, X.; Guo, B. Types of continental shale oil, resource potential and boundary with tight oil in China. *Pet. Explor. Dev.* **2020**, *47*, 1–10. [CrossRef]

8. Du, J.H.; Hu, S.Y.; Pang, Z.L.; Lim, S.; Hou, H.; Zhu, K. Types, potentials and prospects of continental shale oil in China. *China Pet. Explor.* **2019**, *24*, 560–568.
9. Ross, D.J.K.; Bustin, R.M. Characterizing the shale gas resource potential of Devonian-Mississippian strata in the Western Canada sedimentary basin: Application of an integrated formation evaluation. *AAPG Bull.* **2008**, *92*, 87–125. [CrossRef]
10. Yang, Z.; Hou, L.H.; Lin, S.H.; Luo, X.; Zhang, L.; Wu, S.; Huo, J. Geological characteristics and exploration potential of tight oil and shale oil in Lucaogou Formation of Jimsar Sag. *China Pet. Explor.* **2018**, *23*, 76–85.
11. Wang, X.W.; Guan, P.; Liang, X.W.; Ding, X.; You, Y.; Zhang, C.; Feng, S.; Zhang, J. Characteristic Analysis of High Quality Shale Oil Reservoirs in Chang 7 Member of Ordos Basin. *J. Peking Univ. Nat. Sci. Ed.* **2021**, *57*, 459–469.
12. Yang, Z.M.; Jiang, H.Q.; Li, S.T.; Zhu, G. Study on characteristic parameters of microscopic pore structure of low permeability gas reservoirs: Taking Sulige and Dina low permeability reservoirs as examples. *J. Pet. Nat. Gas* **2007**, *29*, 108–110.
13. Zhang, S.; Liu, H.M.; Song, G.Q.; Wang, Y.; Chen, S.; Zhan, S.P. Genesis and controlling factors of shale oil reservoir space in Dongying Sag. *Pet. J.* **2016**, *12*, 1495–1507.
14. Yang, F.; Ning, Z.F.; Hu, C.P.; Wang, B.; Peng, K.; Liu, H. Shale reservoir microscopic pore structure characteristics. *Pet. J.* **2013**, *34*, 301–311.
15. Wei, P.F.; Zhang, J.C.; Long, S.; Peng, J.L.; Deng, E.D.; Lv, Y.N.; Ma, Y.L. Micropore structure and main controlling factors of shale development of Longmaxi Formation in Sichuan Basin and surrounding areas. *China Pet. Explor.* **2016**, *21*, 42–51.
16. Li, W.B.; Jiang, Z.X.; Li, Z.; Chen, Z.; Wang, P. The microscopic pore structure characteristics and control factors of shale in southeast Chongqing. *Spec. Reserv.* **2016**, *23*, 50–54. [CrossRef]
17. Huang, L.; Shen, W. Analysis of pore development characteristics and main controlling factors of shale gas reservoirs: A case study of Longmaxi Formation in Upper Yangtze area. *Geol. Front.* **2015**, *22*, 374–385.
18. Chalmers, G.R.; Bustin, R.M.; Power, I.M. Characterization of gas shale pore systems by porosimetry pycnometry surface area and field emission scanning electron microscopy /transmission electron microscopy image analyses: Examples from the Barnett, Woodford, Haynesville, Marcellus, and Doig units. *AAPG Bulletin* **2012**, *96*, 1099–1119. [CrossRef]
19. Liu, G.H.; Huang, Z.L.; Guo, X.B.; Liu, Z.Z.; Gao, X.Y.; Chen, C.C.; Zhang, C.L.; Wang, X. Occurrence and genesis of SiO_2 in shale series of Middle Permian Lucaogou Formation in Malang Sag, Santanghu Basin, Xinjiang. *Geology* **2016**, *90*, 1220–1235.
20. Si, K.L.; Cao, Y.C.; Zhu, R.K.; Shao, Y.; Xue, X.J.; Wang, X. Rock types and characteristics of tight oil reservoirs of Permian Lucaogou Formation in Jimsar Sag. *Pet. J.* **2015**, *36*, 1495–1507.
21. Huang, S.J.; Huang, K.K.; Feng, W.L.; Tong, H.; Liu, L.; Zhang, X. Material exchange and secondary pore formation between feldspar, kaolinite, and illite during diagenesis: A study from Upper Paleozoic in Ordos Basin and Triassic Xujiahe Formation in Western Sichuan Depression. *Geochemistry* **2009**, *38*, 498–506.
22. Sing, K.S.W.; Everett, D.H.; Haul, R.A.W.; Moscou, L.; Pierotti, R.A.; Rouquerol, J.; Siemieniewska, T. Reporting physisorption data for gas/solid systems with special reference to the determination of surface area and porosity (Recommendations 1984). *Pure Appl. Chem.* **1985**, *57*, 603–619. [CrossRef]
23. Milliken, K.L.; Rudnicki, M.; Awwiller, D.N.; Zhang, T.W. Organic matter-hosted pore system, Marcellus Formation (Devonian), Pennsylvania. *AAPG Bull.* **2013**, *97*, 177–200. [CrossRef]
24. Yu, B.S. Pore classification and characterization of shale gas reservoirs. *Geol. Front.* **2013**, *20*, 211–220.
25. Mastalerz, M.; Schimmelmann, A.; Drobniak, A.; Chen, Y. Porosity of Devonian and Mississippian New Albany Shale across a maturation gradient: Insight from organic petrology, gas adsorption, and mercury intrusion. *AAPG Bull.* **2013**, *97*, 1621–1643. [CrossRef]
26. Wang, X.; Hou, J.; Li, S.; Dou, L.; Song, S.; Kang, Q.; Wang, D. Insight into the nanoscale pore structure of organic-rich shales in the Bakken Formation, USA. *J. Pet. Sci. Eng.* **2020**, *191*, 107–182. [CrossRef]
27. Wu, Y.; Tahmasebi, P.; Lin, C.; Zahid, M.A.; Dong, C.; Golab, A.N.; Ren, L. A comprehensive study on geometric, topological and fractal characterizations of pore systems in low-permeability reservoirs based on SEM, MICP, NMR, and X-ray CT experiments. *Mar. Pet. Geol.* **2019**, *103*, 12–28. [CrossRef]
28. Yang, C.; Zhang, J.C.; Tang, X. Ordos Basin continental shale micro pore type and its influence on shale gas storage and permeability. *Geol. Front.* **2013**, *20*, 240–250.
29. Thyne, G.; Boudreau, B.P.; Ramm, M.; Midtbø, R.E. Simulation of potassium feldspar dissolution and illitization in the Statfjord formation, North Sea. *AAPG Bull.* **2001**, *85*, 621–635.
30. Zhao, P.; Li, X.Q.; Tian, X.W. Micropore structure characteristics of shale gas reservoirs in Longmaxi Formation in southern Sichuan. *Nat. Gas Earth Sci.* **2014**, *25*, 947–956.
31. Loucks, R.G.; Reed, R.M.; Ruppel, S.C.; Hammes, U. Spectrum of pore types and networks in mudrocks and a descriptive classification for matrix-related mudrock pores. *AAPG Bull.* **2012**, *96*, 1071–1098. [CrossRef]
32. Medek, J.; Weishauptová, Z. The microporous phase of carbonaceous substances and its fractal dimension. *Fuel* **2000**, *79*, 1621–1626. [CrossRef]